Showcasing research from Professor Imoto's laboratory, Faculty of Molecular Chemistry and Engineering, Kyoto Institute of Technology, Kyoto, Japan.

Dithienoarsinines: stable and planar π-extended arsabenzenes

Dithienoarsinines, the first π-extended arsabenzenes, exhibit remarkable stability and planarity. This study explores their structure, optical and electronic properties, reactivity, and coordination behavior, highlighting the unique features of arsenic.

As featured in:

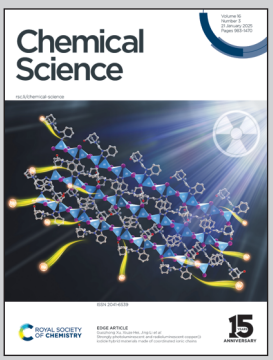

See Hiroaki Imoto *et al.*, *Chem. Sci.*, 2025, **16**, 1126.

ROYAL SOCIETY OF CHEMISTRY

15 YEARS ANNIVERSARY

rsc.li/chemical-science

Registered charity number: 207890

Chemical Science

ROYAL SOCIETY OF CHEMISTRY

EDGE ARTICLE

View Article Online
View Journal | View Issue

Cite this: *Chem. Sci.*, 2025, **16**, 1126

All publication charges for this article have been paid for by the Royal Society of Chemistry

Received 28th September 2024
Accepted 18th November 2024

DOI: 10.1039/d4sc06590e

rsc.li/chemical-science

Dithienoarsinines: stable and planar π-extended arsabenzenes†

Akifumi Sumida,[a] Akinori Saeki,[bc] Kyohei Matsuo,[d] Kensuke Naka[ae] and Hiroaki Imoto[*aef]

Stable planar dithienoarsinines were synthesized and structurally characterized. These compounds exhibit monomeric structures in the solution and solid states, avoiding dimerization, even in the absence of steric protection. They exhibited high global aromaticity with 14 or 22π-electron systems. In the solid state, intermolecular interactions through arsenic atoms were observed, and As···As interactions resulted in aggregation-induced emission enhancement properties with a significant bathochromic shift. The $W(CO)_5$ complex displayed a significantly distorted coordination geometry owing to arsenic cooperative stacking and hydrogen interactions, resulting in a 1D alignment of the complex. Additionally, despite their aromatic nature, dithienoarsinines undergo reactions with alkynes or benzynes to form the corresponding [4 + 2] cycloadducts. Oxygen molecules oxidize the *p*-position of arsinine, leading to the formation of σ-dimerized compounds while retaining the aromaticity of the arsinine ring. In contrast, oxygen attacks the phosphorus atom in phosphinine, resulting in the formation of phosphinic acid with a loss of aromaticity.

Introduction

Since the 1960s, heterobenzenes have attracted significant attention and numerous heteroatoms have been incorporated into benzene frameworks to investigate their structure, aromaticity, and reactivity.[1] Among these, group 15 heterobenzenes, heavier analogs of pyridine, are noteworthy because of their lone pair of electrons, which confer Lewis basicity, and their dicoordinated structure, which maintains planarity (Fig. 1a). Phosphinine motifs are widely utilized as ligands in transition-metal complexes and as conjugated units in organic semiconductors (Fig. 1b).[2] Transition metal complexes with phosphinine ligands have been extensively studied because of their ability to coordinate through various modes. Phosphinine units serve as π-acceptors due to the symmetry and lower energy

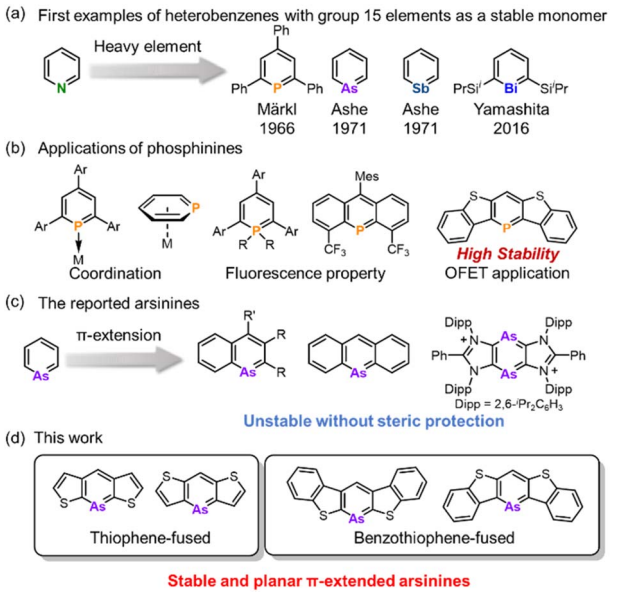

Fig. 1 (a) First examples of the isolation of heterobenzenes embedded with pnictogens as a stable monomer. (b) The applications of phosphinines and π-extended phosphinines. (c) The examples of arsinine derivatives with π-extension. (d) Thiophene- and benzo[*b*]thiophene-fused arsinines.

[a]*Faculty of Molecular Chemistry and Engineering, Graduate School of Science and Technology, Kyoto Institute of Technology, Goshokaido-cho, Matsugasaki, Sakyo-ku, Kyoto 606-0962, Japan. E-mail: himoto@kit.ac.jp*

[b]*Department of Applied Chemistry, Graduate School of Engineering, Osaka University, 2-1 Yamadaoka, Suita, Osaka 565-0871, Japan*

[c]*Innovative Catalysis Science Division, Institute for Open and Transdisciplinary Research Initiatives (ICS-OTRI), Osaka University, 1-1 Yamadaoka, Suita, Osaka 565-0871, Japan*

[d]*Institute for Chemical Research, Kyoto University, Gokasho, Uji, Kyoto 611-0011, Japan*

[e]*Materials Innovation Lab, Kyoto Institute of Technology, Goshokaido-cho, Matsugasaki, Sakyo-ku, Kyoto 606-0962, Japan*

[f]*Fusion Oriented Research for Disruptive Science and Technology (FOREST), Japan Science and Technology Corporation (JST), Honcho 4-1-8, Kawaguchi, Saitama 332-0012, Japan*

† Electronic supplementary information (ESI) available: Synthesis, X-ray data, photophysical properties, reactivity, TRMC, DFT calculations. CCDC 2385300–2385311. For ESI and crystallographic data in CIF or other electronic format see DOI: https://doi.org/10.1039/d4sc06590e

level of their LUMO, as well as σ-donors through their lone pairs. This dual functionality led to the development of unique metal complexes using monodentate and multidentate phosphinine ligands.[2a–c,3] In the realm of luminescent materials, λ^3- and λ^5-phosphinines have been extensively explored,[4] and recently, blue OLED materials based on λ^5-phosphinine have been developed.[5] Additionally, π-extended phosphinines have gained interest for their structure, reactivity, and electronic properties as heavier aromatic molecules and their potential applications in optoelectronics and semiconductors. Consequently, various phosphinine derivatives have been synthesized and investigated, including 1-phosphanaphthalene,[6] 2-phosphanaphthalene,[7] 5-phosphaphenanthrene,[8] phosphaanthracene,[9] 1,4-diphosphinine,[10] and dithieno[3,2-*b*:4,5-*b*′]phosphinine.[11]

In contrast to the rich chemistry of phosphinines, arsinines, which are heavier analogs, have been markedly less studied, and their synthesis remains challenging (Fig. 1c). This is because of the potential instability caused by the poor overlap between the arsenic and carbon orbitals.[12] Conversely, utilizing the large arsenic π-orbital could enhance the intermolecular interaction to construct the unique molecular arrangement. Furthermore, a narrower bandgap can be utilized for luminescent materials or unique reactivities. The parent arsinine was first synthesized by Ashe in 1971,[13] marking the commencement of its chemical investigation, with various derivatives emerging in the 1970s.[14] Despite these developments, its π-extended derivatives are rare. In 1969, Jutzi and Bickelhaupt reported the synthesis of 9-arsaanthracene,[15] although it was detected only by mass spectrometry and UV-vis absorption spectroscopy and was isolated as the [4 + 2] adduct with maleic anhydride. In 2001, Ashe described 1-arsanaphthalene bearing a trimethylsilyl group at the 2-position.[16] Nevertheless, these arsinines are prone to rapid dimerization at ambient temperatures *via* [2 + 2] or [4 + 2] cycloaddition, which hinders detailed structural and property insights. More recently, Dostál synthesized 1-arsanaphthalene from 2,1-benzoazaarsole by incorporating bulky diisopropylphenyl (Dipp) groups.[17] Ghadwal investigated 1,2-diarsinine, which exhibited benzenoid rather than diradical characteristics.[18] However, they feature steric protection groups that are stable in the monomeric state. This poses a significant obstacle to the investigation of reactivity and intermolecular interactions. Therefore, a novel molecular design was developed to circumvent the introduction of sterically protected groups.

Tovar *et al.* reported that benzo[*b*]thiophene-fused borepins exhibited enhanced aromaticity compared to the thiophene-fused variant.[19] The aromaticity of the borepin ring is localized and enhanced according to Clar's aromatic sextet rule. This electronic stabilization strategy was extended to include phosphinines. Yamada *et al.* detailed a benzo[*b*]thieno-fused phosphinine that exhibited stability under ambient conditions owing to the preservation of aromaticity within the phosphinine ring and the distinct isolated aromaticity.[20] Importantly, the absence of steric protection enables their application in field-effect transistor (FET) devices. We envisioned that heavier heterobenzenes could also be stabilized based on the electronic stabilization strategy and that monomeric arsinines with high planarity could be synthesized without any steric protection.

In this study, we synthesized a series of highly planar thiophene- and benzo[*b*]thiophene-fused arsinines (Fig. 1d) that were stable in their monomeric states in solution and solid states, even without steric protection groups. The structures, aromaticity, electronic properties, and reactivities of the π-expanded arsinines were investigated experimentally and computationally.

Results and discussion

The syntheses of thiophene- and benzo[*b*]thiophene-fused arsinines are outlined in Scheme 1. Bis-bromo(benzo[*b*])thienyl methanes **1a–d** were synthesized in 3–4 steps, starting from commercially available thiophenes, and were isolated in moderate yields without the need for column chromatography. Bromine–lithium exchange reactions with **1a–d** were conducted by treatment with *n*-butyllithium (*n*-BuLi), followed by a reaction with dimethyltin dichloride (Me_2SnCl_2) to yield the corresponding tin precursors **2a–d**. Benzo[*b*]thieno-fused tin compounds **2c** and **2d**, which are stable under ambient conditions (air and light), were purified by trituration with ethanol and subjected to silica gel column chromatography. In contrast, thieno-fused tin compounds **2a** and **2b** were slightly sensitive and underwent hydrolysis during passing through neutral silica/alumina gel column chromatography (Fig. S10†). The crude products of **2a** and **2b** with sufficient purity were used in subsequent steps after removing the inorganic salts. Following the tin–arsenic exchange of **3a–d** with arsenic tribromide ($AsBr_3$) in benzene or tetrahydrofuran (THF) at 50 °C, three equivalents of 1,8-diazabicyclo[5.4.0]undec-7-ene were reacted. After solvent evaporation, **3c** and **3d** were triturated with ethanol in air, whereas **3a** and **3b** were isolated under argon atmosphere. Benzo[*b*]thieno-fused phosphinine **3c-P** was also synthesized by replacing $AsBr_3$ with phosphorus tribromide (PBr_3), and **3d-P**, a phosphorus analog of **3d**, was prepared according to the literature.[20] All the arsinines

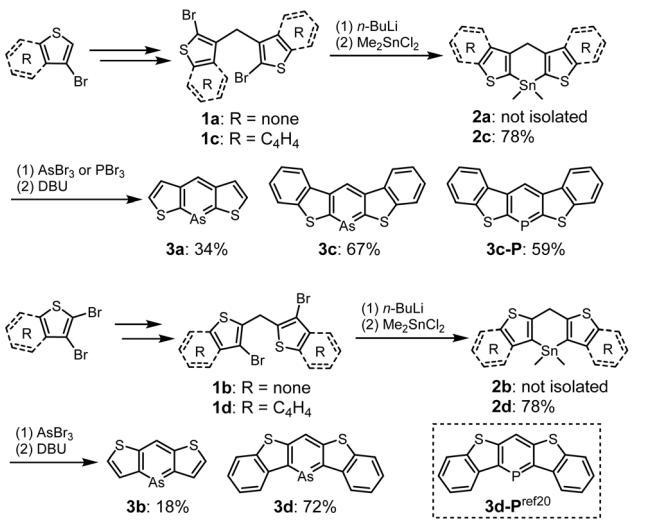

Scheme 1 Synthesis of **3a–d** and **3c-P**.

and phosphinines were characterized using NMR, HR-MS, and single-crystal X-ray analysis. In the ^{1}H-NMR spectra, signals attributed to the benzylic protons of **2** at approximately 5.4 ppm disappeared, and a singlet peak that shifted to 8 ppm appeared, assigned to the proton at the 4-position of the arsinines (Fig. S11†). In the ^{13}C-NMR spectra, the benzylic carbon signals shifted to the aromatic region (Fig. S12†). The ^{1}H- and ^{13}C-NMR spectra confirmed that all the arsinines and phosphinines exhibited high aromaticity, indicating their monomeric structure in the solution state, with no dimeric compounds detected. Although **3c** and **3d** were stable in solid form, they were slightly unstable to oxygen in solution and insoluble solids precipitated after storage in air for several days (*vide infra*). All arsinines **3a–d** have photostability and can be stored under light in solution and solid state. In addition, thermal stabilities of air-stable arsinines **3c** and **3d** were evaluated by thermal gravimetric analysis (TGA) under nitrogen atmosphere (Fig. S15†). They have high thermal stabilities considering that their decomposition temperatures at 5 wt% loss (T_{d5}) were 285 °C (**3c**) and 272 °C (**3d**).

Single-crystal X-ray diffraction was used to obtain structural information. Single crystals of **3a–d** were obtained by slowly diffusing ethanol into dichloromethane solutions of **3a**, **3b**, and **3d**, or by slowly cooling chlorobenzene solutions of **3c** and **3c-P**. Two polymorphs of **3d** were obtained and characterized as plate (major) and needle (minor) crystals. The plate polymorph exhibited sandwich herringbone packing, whereas the needle polymorph displayed the same 1D-columnar packing as the previously reported **3d-P**. The crystal data for **3b** and **3d** (plate) indicate disordered structures with flipped molecules, suggesting that a detailed discussion of the structural parameters might be inappropriate. Photophysical and carrier mobility data were collected for **3d** (plate) in the present study (*vide infra*). All arsinines demonstrated monomeric structures in the solution and solid states, as determined from the NMR spectra and X-ray data, respectively. The structures of **3a**, **3c**, and **3d** (needle) are shown in Fig. 2 (for other structures, see ESI†), and the structural parameters of **3a**, **3c**, **3d** (needle), **3c-P**, **3d-P**, and the carbon analog of **3d** (**4**) are summarized in Tables 1 and 2. The arsenic atoms in these structures were dicoordinated with C1–As–C5 angles of 94.7(2)°, 94.8(2)°, and 97.4(2)°, respectively. The arsinine rings are highly planar, and the sum of the internal angles in the arsinine rings is 719.9° (**3a**), 720.0° (**3c**), and 720.0° (**3d**). Regarding the overall planarity of the molecules, the root mean square deviations (RMSD) from the mean plane of the entire molecule were 0.025 Å (**3a**), 0.051 Å (**3c**), and 0.029 Å (**3d**). The dihedral angles between the two terminal thiophene (**3a**) and benzene (**3c** and **3d**) rings were 2.77°, 4.29°, and 3.01°, respectively, indicating high planarity but slight twisting with increased π-extension. Focusing on elements such as carbon and phosphorus, it was observed that the C–E–C angles decreased in the order of C (**4**, 119.3(4)°), P (**3d-P**, 100.5(1)°), and As (**3d**, 97.4(2)°), and the dihedral angles and RMSD values decreased in the order of C (**4**, 0.067 Å), As (**3d**, 0.029 Å), and P (**3d-P**, 0.026 Å). Furthermore, **3c** (RMSD = 0.051 Å) exhibited

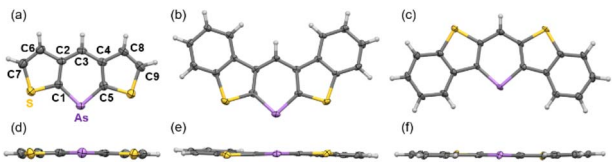

Fig. 2 ORTEP of (a and d) **3a**, (b and e) **3c**, and (c and f) **3d**. Thermal ellipsoids are drawn at the 50% probability level.

Table 2 Bond length (SC-XRD analysis) and WBIs (optimized structure) of **3a**, **3c**, **3d**, **3c-P**, **3d-P** and **4**. The label for numbering atoms is shown in Fig. 2

	C–E bond/Å (WBI)	C(1/5)–S bond/Å (WBI)	C(7/9)–S bond/Å (WBI)
3a	1.860(3)	1.738(3)	1.727(4)
	1.859(3)	1.728(3)	1.736(4)
	(1.22)	(1.17)	(1.16)
3c	1.853(5)	1.743(5)	1.762(4)
	1.864(5)	1.756(4)	1.757(5)
	(1.22)	(1.15)	(1.11)
3d	1.857(5)	1.763(4)	1.742(5)
	1.859(5)	1.769(5)	1.752(5)
	(1.21)	(1.12)	(1.09)
3c-P	1.739(2)	1.752(2)	1.744(2)
	1.740(2)	1.755(2)	1.750(2)
	(1.24)	(1.16)	(1.10)
3d-P[20]	1.737(2)	1.755(3)	1.751(3)
	1.732(3)	1.760(2)	1.741(3)
	(1.26)	(1.10)	(1.10)
4[20]	1.393(6)	1.753(4)	1.755(4)
	1.394(6)	1.753(4)	1.755(4)
	(1.40)	(1.11)	(1.10)

Table 1 Structural data from SC-XRD analysis of **3a**, **3c**, **3d**, **3c-P**, and **3d-P**

	C1–E–C5 angle/°	Sum of inner angle[a]/°	Dihedral angle[b]/°	RMSD[c]/Å
3a	94.7(2)	719.9	2.77	0.025
3c	94.8(2)	720.0	4.29	0.051
3d	97.4(2)	720.0	3.01	0.029
3c-P	97.63(9)	720.0	3.38	0.042
3d-P[20]	100.5(1)	720.0	2.62	0.026
4[20]	119.3(4)	720.0	7.42	0.067

[a] Sum of the inner angles of the arsinine/phosphinine ring. [b] Dihedral angles between the two thiophenes in **3a** and benzenes in **3c**, **3d**, **3c-P**, **3d-P** and **4**. [c] Root mean square deviation from the mean plane.

larger values compared to **3d**, a trend similarly observed in their phosphorus analogs (**3c-P** > **3d-P**). In **3d-P**, the strain induced by thiophene ring contraction was mitigated by the longer C–P bond, enhancing the planarity. However, in the case of arsenic, an increased C–As bond length led to reduced planarity. Additionally, in terms of fused-ring patterns, the planarity in **3c**/**3c-P** was further decreased compared to **3d**/**3d-P** because of steric repulsion between the protons on the benzene ring and the proton at C3.

The bond lengths within the ring provided important insights into aromaticity, and we focused on the C–C, As–C, and S–C bonds. The As–C bond lengths ranged from 1.853 to 1.864 Å, positioned between the typical ranges for single (1.946–1.964 Å in triphenylarsine)[21] and double bonds (1.816–1.827 Å in non-conjugated acyclic arsaalkenes).[22] These lengths are comparable to those reported for arsinines, such as 1-arsanaphthalene (1.832 to 1.893 Å)[17] and 1,4-diarsinine (1.856–1.877 Å).[18] No differences in the As–C or P–C bond lengths were observed between the two thiophene fusion modes. The C–C bond lengths within the arsinine rings varied from 1.388 to 1.430 Å, with no significant differences between compounds **3a** and **3c**. The C–S bond lengths between arsinine and thiophene increased from **3a** to **3c**, and the two modes of thiophene fusion (**3c**/**3d**) caused little variation in these lengths. The Wiberg bond indices (WBIs) based on the optimized structures (B3LYP/def2TZVP) confirmed these tendencies. These findings suggest that the aromaticity of the arsinine rings remained consistent even after the π-extension, whereas the aromaticity of the thiophene decreased.

For further understanding of aromaticity, nucleus-independent chemical shift (NICS) analysis[23] (GIAO-B3LYP/def2TZVP) was conducted to assess the aromaticity of compounds **3a–d** (Fig. 3a). The benzene value (−29.8 ppm) showed that all arsinine rings exhibited sufficient aromaticity, ranging from −20.9 to −23.1 ppm. The NICS 1D plots of **3a–d** displayed typical aromatic characteristics similar to those of the benzene rings in **3c** and **3d**, which also showed high aromaticity (Fig. S18a–S21a†). However, the values for thiophene differed by the π-extension. **3a** and **3b** exhibited −25.1 and −24.9 ppm, respectively, indicating high aromaticity, whereas **3c** and **3d** showed significantly lower values (−14.2 ppm and −13.6 ppm, respectively), indicating weakened aromaticity in the fused thiophene. This was consistent with the results of the X-ray crystal analysis. The NICS-XY scan[24] (Fig. S18b–S21b†) revealed that, although **3a** and **3b** had three local circuits at the thiophenes and arsinine, **3c** and **3d** had three aromatic circuits at the benzenes and arsinines. Similar observations have been reported for benzo[*b*]thiophene-fused borepins,[19] in which the arsinine rings of **3c** and **3d** exhibit isolated aromaticity. The phosphinine ring in **3c-P** showed higher aromaticity (−23.1 ppm, Fig. S22–S23†) than that of the arsinines, although the NICS(1)$_{zz}$ values for the thiophene and benzene rings of **3c-P** (−13.6 and −27.6 ppm, respectively) were similar to those of **3c**. The major resonance structures of **3a** and **3b** were localized on thiophene and arsinine, whereas those of **3c** and **3d** were localized only on arsinine and the two benzene rings (Fig. 3b). To further investigate the aromaticity of **3a–d**, an anisotropically induced current density (ACID) analysis (CSGT-B3LYP/def2TZVP) was performed (Fig. 3c).[25] The ACID plots revealed that arsinines **3a–d** and phosphinine **3c-P** (Fig. S24†) demonstrated clockwise currents at the periphery of the molecule, indicating global aromaticity and a 14 (**3a** and **3b**) or 22π (**3c** and **3d**) electron aromatic system. Additionally, focusing on the As–C moieties, it was observed that π-electron delocalization was diminished due to weak overlap between the 4p orbital of arsenic and the 2p orbital of carbon. Notably, this represents the first example of a stable 14 or 22π-electron arsinine synthesis.

To determine the electronic structures of arsinines **3a–d** and phosphinine **3c-P**, their absorption/emission spectra were measured in 2-methyltetrahydrofuran (2-MeTHF) solution and are summarized in Fig. 4 and Table 3. Arsinines and phosphinines exhibited two absorption bands in the 280–320 nm and 350–400 nm ranges, respectively. The substitution patterns had a minimal effect on the optical properties of the monomeric states, with a slight red-shift from **3a** to **3c** or **3b** to **3d**. The longest absorption maxima (λ_{abs}) of **3a** and **3c** were red-shifted due to the expanded conjugation. Furthermore, in examining the effect of π-extension by comparing **3c** and **3d** the absorption wavelengths were also red-shifted.

To elucidate the origin of the absorption, time-dependent DFT (TD-DFT) calculations were conducted at the B3LYP/

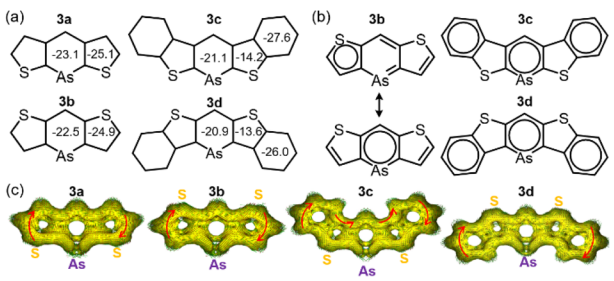

Fig. 3 Aromaticity evaluations: (a) NICS(1)$_{zz}$ values of **3a–d**. (b) Clar's sextet of major resonance structures of **3a**, **3c**, and **3d**. (c) ACID plots of **3a–d**.

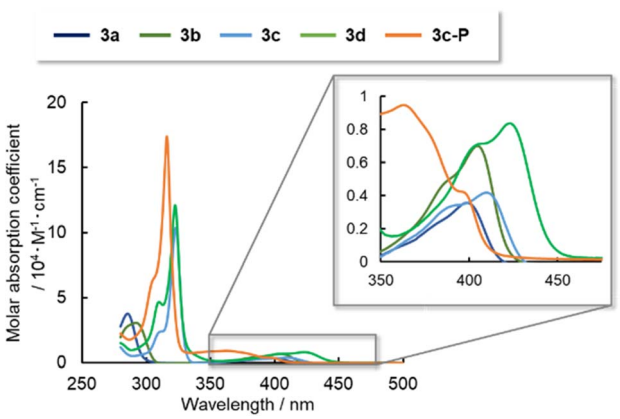

Fig. 4 UV-vis absorption spectra of **3a–d** and **3c-P** in 2-MeTHF solutions (1.0×10^{-5} M).

Table 3 Photophysical properties of **3a–d** and **3c-P** in solutions[a]

			298 K				77 K		
	λ_{abs}[b] [nm]	ε[c] [M^{-1} cm^{-1}]	λ_{ex}[d] [nm]	λ_{em}[e] [nm]	Φ[f]	τ[g]	λ_{em}[e] [nm]	Φ[f]	τ[g]
3a	400	3500	286	424	0.02	53.4 ns	420	0.89	12.7 ns
3b	404	6200	—	n.d.	n.d.	n.d.	n.d.	n.d.	n.d.
3c	410	4200	322	440	<0.01	1.0 ns	430, 668	0.01, 0.08	0.71 ns, 1.1 ms
3d	422	8400	322	455	0.02	1.3 ns	440, 570	0.04	2.1 ns, 35 ms
3c-P	398	4000	316	420	0.01	34.3 ns	390, 575	0.06, 0.12	36.8 ns, 127 ms

[a] Measured in 2-MeTHF (1.0×10^{-4} M for **3a–b**, 1.0×10^{-5} M for **3c–d** and **3c-P**) solutions. [b] The longest absorption maxima. [c] Molar excitation coefficients at the absorption maxima. [d] Excitation maxima monitored at the emission maxima. [e] Emission maxima monitored at the excitation maxima. [f] Absolute quantum yield. [g] Emission lifetime.

def2TZVP level of theory, and the orbital distributions and energy levels are summarized in Fig. 5. The electronic transitions of all compounds were attributed to the HOMO–LUMO transitions, with the oscillator strengths of **3a–d** estimated to be small (f = 0.0162–0.0715). Regarding the orbital levels, the HOMO and LUMO were stabilized after the π-extension from **3a** to **3c**. The delocalization of the LUMO stabilized the LUMO, whereas the stabilization of the HOMO was attributed to the stabilizing effect of the Clar's sextets in the outer benzene rings, thus lowering the HOMO level owing to the aromatic stabilization energy.[26] In view of the differences in substitution patterns between **3c** and **3d**, the changes had minimal effect on the HOMO, whereas the LUMO was stabilized by 0.24 eV due to the increased delocalization. When substituting arsenic for phosphorus, the orbital distributions remained almost the same; however, the bandgap was narrowed due to the smaller energy splitting of π–π* because of the poor overlaps between carbon and the heavier atom. Furthermore, the spatial distribution of the orbitals of **3c** compared to those of **3c-P** may enhance the intermolecular interactions through the arsenic atoms.[27]

Photoluminescence (PL) spectra were obtained for solution and solid states. In solution, all the compounds except **3b** exhibited fluorescence spectra, with the order of the fluorescence wavelengths being consistent with the order of their absorption wavelengths (Fig. 6a). For **3b**, the small energy gap between S_1 and T_2 (0.003 eV) might promoted the intersystem crossing (Fig. S26†). The triplet excitons were deactivated *via* non-radiative pathway probably because the large energy gap between T_2 and T_1 (1.51 eV) inhibited the internal conversion. The emission lifetimes (τ) were ns-order at 298 K, implying that the emissions were fluorescence. No excimer emissions were observed even at higher concentrations (1.0×10^{-3} M for **3a**, 1.0×10^{-4} M for **3c**, **3d**, **3c-P**). The quantum yields were <0.02, as the oscillator strengths of the $S_0 \rightarrow S_1$ transitions were small due to the partial change in orbital symmetry. Low fluorescence efficiencies were observed in λ^3-phosphinines due to the low differences of symmetry between the HOMO and LUMO.[4] Additionally, PL spectra were measured in a glass matrix of 2-MeTHF at 77 K (Fig. 6b). Although **3a** showed only fluorescence even at 77 K, the benzothiophene-fused compounds **3c**, **3d**, and **3c-P** displayed fluorescence and phosphorescence, judging from the co-existence of the ns- and ms-order τ values. DFT analysis revealed that the T_2 levels of **3c**, **3d**, and **3c-P** were less than their S_1 levels, and their energy gaps between the T_2 and S_1 were sufficiently small (**3c:** 0.34 eV, **3d:** 0.23 eV, **3c-P:** 0.37 eV) to promote intersystem crossing, resulting in phosphorescence. In contrast, the T_2 level of **3a** was higher than the T_1 level, and the energy gap between T_1 and S_1 was excessively large (1.45 eV), inhibiting phosphorescence. The low-lying T_2 of **3c**, **3d**, and **3c-P** was probably due to delocalization along the relatively large conjugated system.

In the solid state, although **3a**, **3b**, **3d**, and **3d-P** showed negligible emission, **3c** and **3c-P** exhibited intense red and yellow emissions, respectively (Fig. 7a and b), in contrast to their behavior in solution. The absorption and emission spectra

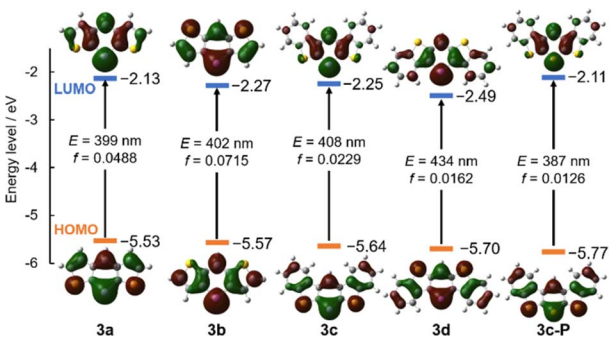

Fig. 5 Frontier orbitals of **3a–d** and **3c-P**, their energy levels, transition energy (E), and oscillator strength (f) for the HOMO–LUMO transitions. Isovalue = 0.025.

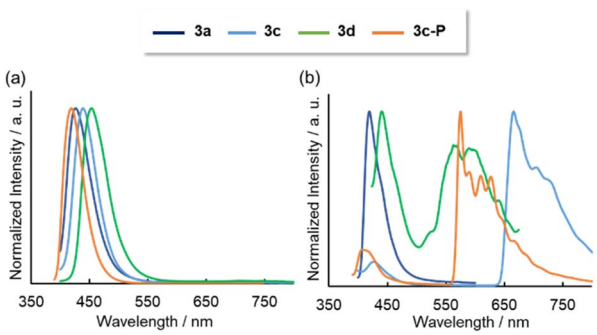

Fig. 6 Emission spectra of **3a–d** and **3c-P** in 2-MeTHF solutions (1.0×10^{-5} M) at (a) 298 K and (b) 77 K.

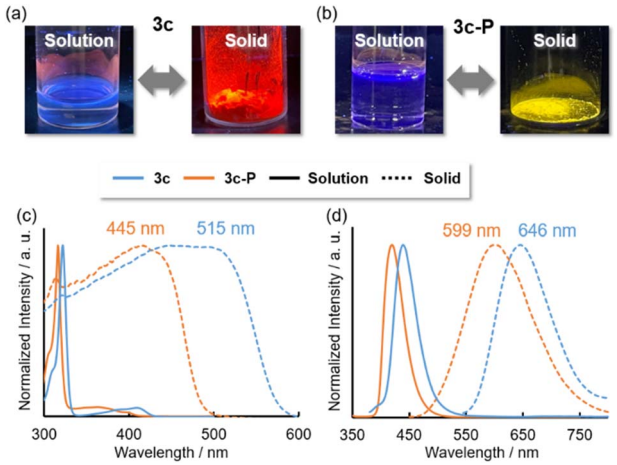

Fig. 7 Pictures of luminescence in solution and solid state of (a) **3c** and (b) **3c-P**. (c) Absorption and (d) emission spectra of **3c** and **3c-P** in solution (solid lines) and solid state (dashed lines).

are shown in Fig. 7c and d, respectively. Significant redshifts were observed for both compounds, accompanied by a broadening of the spectra. The ns-order τ values of **3c** and **3c-P** (0.53 and 1.6 ns, respectively) indicated that the long-wavelength emissions in the solid states were attributed to fluorescence.

To understand the solid-state emission behavior of **3c** and **3c-P**, their packing structures were investigated; for non-emissive solid samples (**3a**, **3b**, and **3d**), please see ESI (Fig. S1–S4†). **3c** and **3c-P** exhibited similar columnar packing structures (Fig. 8a and b) with numerous intermolecular interactions through the π plane (for dimers d_1–d_3) and H···S interactions (Fig. 8c and d). Notably, As···As (**3c**) and P···P (**3c-P**) interactions (for dimer d_4) were observed at distances of 3.500 Å and 3.525 Å, respectively. Although the atomic radius of arsenic (1.85 Å) is larger than that of phosphorus (1.80 Å),[28] the As···As distance was shorter than the P···P distance. This indicates stronger interactions of d_4 in **3c** due to the more spatially expanded molecular orbitals involving the 4p orbital of arsenic, which promotes efficient As···As interaction. The symmetry-adapted perturbation theory (SAPT) was employed to reveal the interaction energies and components, as summarized in Table 4.[29] For the C···C stacked dimer (d_1 and d_3), there were few differences in composed energies between **3c** and **3c-P**. Conversely, in the π-stacked dimer interacting with As or P (d_2), **3c** exhibited closer interaction (3.474 Å) than **3c-P** (3.491 Å), with electrostatic (E_{elst}) and dispersion (E_{disp}) energies (−10.5 and −25.8 kcal mol^{-1}, respectively), more favorable than those of **3c-P** (−8.05 and −23.7 kcal mol^{-1}, respectively). This indicates that the more spatially enlarged arsenic orbitals contribute significantly to intermolecular interactions. For the Pn···Pn interaction (d_4), E_{disp} was the dominant component, with E_{elst} also contributing. The d_4 in **3c** displayed higher E_{disp} and E_{elst} values than those in **3c-P** due to its more spatially expanded orbitals and natural population analysis charge, as confirmed by DFT calculations (Table S18†). However, the short As···As the distance of **3c** resulted in greater destabilization due to exchange energy (E_{exch} = 13.2 kcal mol^{-1}), making the E_{total} (−4.76 kcal mol^{-1}) lower than that of **3c-P** (−4.94 kcal mol^{-1}).

TD-DFT calculations with a dispersion-corrected function (M06/def2-TZVP) were conducted to investigate the reasons for the bathochromic shift and the aggregation-induced emission enhancement (AIEE) properties in selected dimers with π–π (d_1–d_3) or As···As (d_4) interactions (Table S19†). At this calculation level, the transition energy of **3c** was estimated to be 400.7 nm with a small oscillator strength (f = 0.0266). Dimers d_1–d_3 with π–π stacking showed slightly bathochromic shifts from the monomeric state (401.9–423.6 nm); however, their oscillator strengths were still small (0.0126–0.0772). In contrast, dimer d_4 exhibited a bathochromic shift (475.6 nm) and a large oscillator strength (0.2039). For dimer d_4, the HOMO and LUMO levels increased and decreased, respectively. Furthermore, the transition dipole moment of d_4 increased compared to that of the monomeric state because of the symmetry-allowed transitions of the HOMO and LUMO, thereby facilitating the S_0 and S_1 transitions of **3c** and **3c-P**. Consequently, **3c** and **3c-P** exhibited enhanced fluorescence. The Pn···Pn interaction for d_4 resulted in AIEE properties, as these compounds showed more efficient fluorescence (Φ = 0.10 and 0.18, respectively) in the solid state than in the solution state (Φ = 0.01).

We then evaluated the hole mobilities of **3c**, **3d**, and **3c-P** by conducting flash photolysis time-resolved microwave conductivity (TRMC) measurements (Fig. S16 and S17†).[30] Photocarriers were generated by excitation at 355 nm. The TRMC

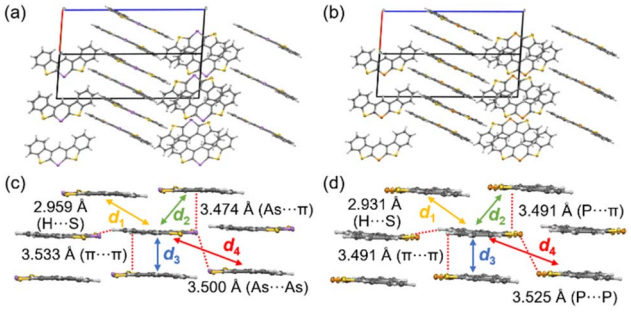

Fig. 8 Packing structures of (a) **3c** and (b) **3c-P**. Intermolecular interactions of (c) **3c** and (d) **3c-P** with showing dimers d_1–d_4.

Table 4 SAPT analysis (SAPT0/jun-cc-PVDZ) of the selected dimer of **3c** and **3c-P** in the solid state

		E_{elst}[a]	E_{exch}[b]	E_{ind}[c]	E_{disp}[d]	E_{total}[e]
3c	d_1	−5.89	8.72	−1.19	−12.3	−10.6
	d_2	−10.5	21.6	−2.11	−25.8	−16.8
	d_3	−11.0	25.1	−2.58	−35.5	−24.0
	d_4	−5.78	13.2	−2.39	−9.83	−4.76
3c-P	d_1	−6.40	9.97	−1.33	−12.9	−10.7
	d_2	−8.05	17.5	−1.69	−23.7	−15.9
	d_3	−12.0	27.1	−2.73	−36.5	−24.1
	d_4	−3.50	9.18	−1.55	−9.08	−4.94

[a] Electrostatic. [b] Exchange. [c] Induction. [d] Dispersion. [e] Total energies (kcal mol^{-1}).

profiles are shown in Fig. S16,† where $\varphi\Sigma\mu$ is the product of φ (the quantum yield of photogenerated charge carriers) and $\Sigma\mu$ (the sum of charge carrier mobilities). The order of $\varphi\Sigma\mu$ maxima was as follows: **3d** (4.3×10^{-5} cm^2 V^{-1} s^{-1}), **3c-P** (3.7×10^{-5} cm^2 V^{-1} s^{-1}), **3c** (2.4×10^{-5} cm^2 V^{-1} s^{-1}), and **3d-P** (1.7×10^{-5} cm^2 V^{-1} s^{-1}). Moreover, the effective lifetime of the TRMC decay was longest for **3d** (4.0 μs) followed by **3c-P** (2.0 μs) and **3c** (1.6 μs), exhibiting the superior photoconductive character of **3d**; the lifetime of **3d-P** was not determined because of the weak signal. Transfer integrals and reorganization energies were calculated for **3c** and **3c-P**, whereas calculations for **3d** were not conducted because of their disordered structures (Table S9†). Although the $\varphi\Sigma\mu$ values were lower than those of typical thienoacenes,[31] the transfer integrals through d_4 dimer showed considerably higher values (176.0 meV) despite their small interaction surface (Table S21†). This is due to their large orbital coefficients and extensive orbitals. Thus, these theoretical evaluations provide insights into novel molecular designs involving acenes embedded with heavy pnictogens for OFET applications with potential charge transport abilities.[32]

The reactivities of the arsinines were also investigated. Heterobenzenes are known to undergo [4 + 2] or [2 + 2] cycloadditions with themselves and with dienes and alkynes.[33] Compounds **3a–d** were reacted with dimethyl acetylenedicarboxylate (DMAD), a dienophile, to yield the [4 + 2] cycloadducts, arsabarrelenes **3-DMAD** (Scheme 2a). In addition, compounds **3a** and **3c** reacted with *o*-benzyne to yield **3a-benzyne** and **3c-benzyne**, respectively (Scheme 2b). The structures of these cycloadducts were characterized using NMR spectroscopy and, for some compounds, using single-crystal X-ray diffraction (Scheme 2c). Furthermore, the thermal activities of the compounds were investigated. Degassed chlorobenzene solutions of **3a–d** were heated to reflux under N_2 atmosphere, and no dimerized products were detected by ^{1}H-NMR spectroscopy.

The complexation behavior was investigated. Arsines have a lone pair with high s-character and less directional coordination behavior.[34] It was assumed that unique molecular arrangements could be achieved by the flexible coordination of arsines and intermolecular interactions through large arsenic orbitals. First, we attempted to synthesize gold(I) complexes by reacting **3d** with gold(I) chloride (AuCl). However, insoluble materials and gold nanoparticles were generated. This probably occurred because Au(I) oxidizes **3d**, reducing it to Au(0) (*vide infra*). Therefore, tungsten hexacarbonyl ($W(CO)_6$) was selected as a redox-neutral metal source. The reaction with **3d** failed due to the low solubility of the complex, resulting in an insoluble material. Thus, **3a** reacted with $W(CO)_6$ because of its better solubility than **3d**.

After recrystallization from THF/hexane, yellow crystals suitable for X-ray structural analysis were obtained. Owing to poor data, the precise parameters of the C–C bonds are not discussed. Surprisingly, the $W(CO)_5$ moiety was tilted 15.27° from the arsinine plane (Fig. 9a and b). To the best of our knowledge, this coordination geometry is the first example of μ^1-coordination in phosphinines and arsinines. NBO analysis revealed that the hybridization of the lone pair comprised 72% 4s orbitals and 28% 4p orbitals for **3a**. Considering the values for triphenylarsine (60% 4s and 40% 4p), pyridine (29% 2s and 71% 2p), and phosphinine (61% 3s and 39% 3p, Table S18†), the lone pair of **3a** had fewer directional orbitals, thus enabling flexible coordination. To elucidate the differences in the coordination behaviors of the pnictogens (N, P, and As), the energy profiles dependent on the coordination angle were calculated (Fig. S27†). The most stable geometries for all elements were planar, with nitrogen and phosphorus showing energies 1.64 and 1.26 kcal mol^{-1} higher, respectively, at 18° than at 0°. In contrast, arsenic showed an energy increase of 0.44 kcal mol^{-1} at 18°, indicating that attractive interactions, such as hydrogen bonds and π–π interactions, can induce the flexible coordination geometry of **3a-W(CO)$_5$**. The optimized structure of **3a-W(CO)$_5$** (B3LYP-GD3BJ/def2-TZVP) showed planar coordination

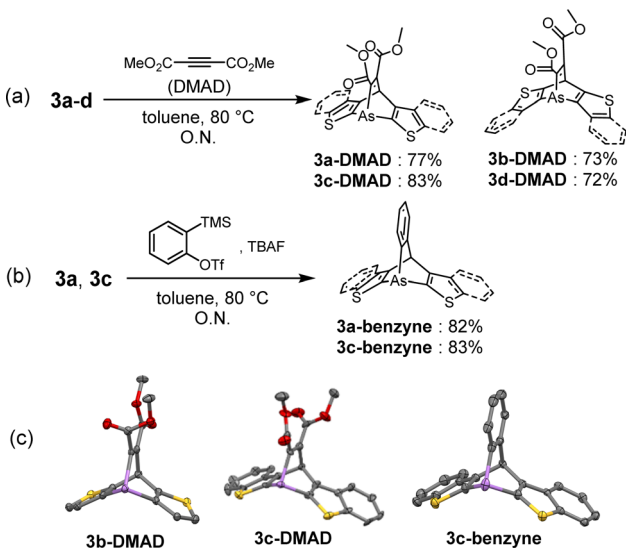

Scheme 2 [4 + 2] cycloaddition of arsinines with (a) dimethylacetylene dicarboxylate (DMAD) (for **3a–d**) and (b) *o*-benzyne (for **3a** and **3c**). (c) ORTEPs of **3b-DMAD**, **3c-DMAD**, and **3c-benzyne**. Thermal ellipsoids are drawn at the 50% probability level. Hydrogen atoms were omitted for clarity.

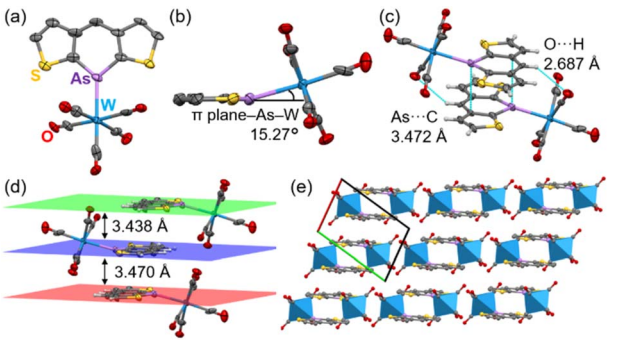

Fig. 9 Crystal structure of **3a-W(CO)$_5$**. (a) Front and (b) side view of **3a-W(CO)$_5$**. (c) Face-to-face stacking dimer, (d) mean planes of each column, and (e) 1D-columnar packing separated by $W(CO)_5$ moiety (blue hexagon).

geometry, suggesting that the distorted coordination direction was caused by intermolecular interactions in the crystal packing. **3a-W(CO)$_5$** exhibited face-to-face stacking with distances of 3.470 Å and 3.438 Å between the mean planes (Fig. 9d). The π–π interactions included As···C interactions at 3.472 Å due to the large arsenic orbitals. Additionally, hydrogen bonds between the carbonyl oxygen and the hydrogen at the 4-position of arsinine at 2.678 Å in each column contributed to the distortion of the As–W coordination (Fig. 9c). Furthermore, **3a-W(CO)$_5$** formed a 1D-columnar packing, with each column separated by the W(CO)$_5$ moiety (Fig. 9e). The optimization of the **3a-W(CO)$_5$** dimer (B3LYP-GD3BJ/def2TZVP) reproduced a distorted structure with a distortion angle of 14.30° (Fig. S28†). Hydrogen bonds and π–π interactions were also confirmed by non-covalent interaction analysis based on the optimized structure (Fig. S29†).[35]

Finally, we investigated the reactivity towards oxygen (O_2) for compounds **3d** and **3d-P** (Scheme 3). As mentioned above, **3d** was slightly unstable to oxygen in solution; insoluble solids precipitated after storage in air for several days even under dark condition. When a solution of **3d** was exposed to air, brown crystals were formed. X-ray structural analysis and ^{1}H-NMR revealed that **3d** dimerized at the 4-position *via* a single bond to form **3d′** (Scheme 3a and e). Based on the bond lengths and NICS(1)$_{zz}$ value of the arsinine ring (−20.9 ppm), **3d** underwent dehydrogenative-oxidative dimerization while retaining its aromaticity. In contrast, the exposure of **3d-P** to air resulted in the precipitation of insoluble materials that could not be analyzed using NMR. Heating a solution of **3d-P** in air yielded a single crystal of the oxidative decomposition product, which was identified as the dimerized phosphinic anhydride **3d-P′** (Scheme 3b and e). Owing to the poor quality of the crystal, the detailed structural parameters are not discussed. The bond lengths in the P-containing six-membered rings exhibit bond alternation. The two P–O bonds had distinct characteristics; the dangling P–O bond was shorter than the bridging P–O bond, indicating that **3d-P′** is a phosphinic acid. Based on the NICS values of **3d** and **3d-P** in the optimized structures, the aromaticity of arsinine was lower than that of phosphinine. However, arsinine **3d** dimerized while retaining its aromaticity, whereas phosphinine **3d-P′** lost its aromaticity. Plausible mechanisms for the oxidative dimerization of **3d** and **3d-P** are shown in Scheme 3c and d, respectively. In **3d**, O_2 initially abstracted hydrogen at the 4-position, and the resulting arsinine radical dimerized. The hydroxyl radicals then abstract hydrogen again, yielding arsinine dimer **3d′**. Other oxidants such as AuCl (*vide supra*), *N*-bromosuccinimide, *N*-iodosuccinimide, and iodine also induced the dimerization of **3d** to **3d′** (Fig. S13 and S14†). For phosphinine **3d-P**, O_2 first attacks the phosphorus atom, generating phosphinine oxide. This intermediate, known for its high instability,[36] reacts with water to form phosphinic acid, which is subsequently dehydrated to yield phosphinic anhydride **3d-P′**. These differences in the oxidative products arise from the intrinsic properties of the elements. Arsinine has lower aromaticity and oxophilicity, allowing O_2 to attack the most reactive hydrogen instead of the arsenic atom. In contrast, phosphinine, which has higher aromaticity and oxophilicity, experiences oxygen attack at the phosphorus atom rather than the hydrogen in the phosphinine ring.

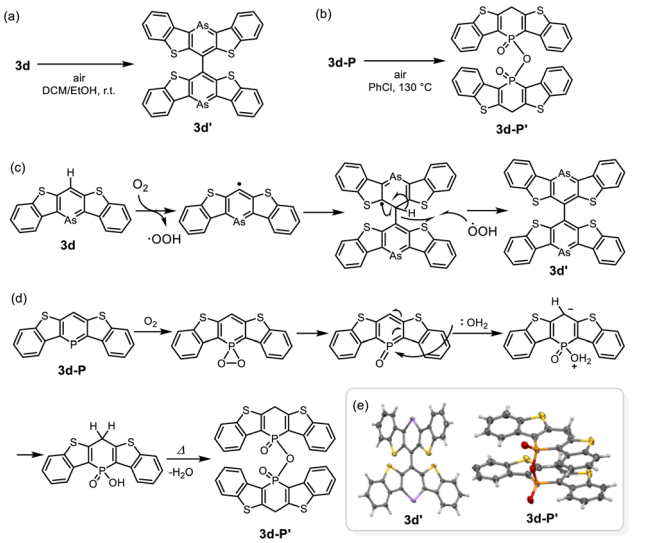

Scheme 3 Dimerization of (a) **3d** and (b) **3d-P** in air, and their plausible mechanisms for (c) **3d** and (d) **3d-P**. (e) ORTEPs of **3d′** and **3d-P′**. Thermal ellipsoids are drawn at the 50% probability level.

Conclusions

We successfully synthesized thiophene- and benzo[*b*]thiophene-fused arsinines (**3a–d**), marking the first instance of stable and planar π-extended arsinines. These compounds exhibited remarkable planarity and bond equalization, including the As–C bonds. NICS and ACID analyses confirmed their 14- or 22π global aromaticity, although the degree of local aromaticity varied depending on the fused rings. The absorption and PL spectra of these arsinines were bathochromically shifted relative to those of their phosphinine analogs (**3c-P** and **3d-P**), which was attributed to the incorporation of heavier pnictogen atoms in the heterocycles. Notably, compound **3c** demonstrated emission enhancement with a significant bathochromic shift in the solid state, compared to its solution-phase emission, due to dimer formation through As···As interactions. The tungsten(0) complexes **3a-W(CO)$_5$** exhibited highly distorted As···W coordination in the solid state, influenced by the less directional lone pair of the As atom and 1D columnar molecular packing. Additionally, [4 + 2] cycloadditions of **3c** and **3d** with alkynes and benzynes were observed. Under an O_2 atmosphere, **3d** dimerized at the 4-position while retaining its aromaticity, whereas the P atom in **3d-P** underwent oxidation, losing its aromaticity, which was driven by their differing affinities for oxygen. This study provides critical insights into the structural, electronic, coordination, and reactivity properties of heavier element-containing heterobenzenes obtained from stable and planar arsinines. Ongoing efforts are directed towards further diversifying and exploring applications of π-extended arsinines.

Data availability

The authors confirm that the data supporting the findings of this study are available within the article and its ESI.†

Author contributions

A. Sumida: synthesis, structural analysis, data curation, writing – original draft; A. Saeki: TRMC measurements, data curation, writing – review and editing; K. Matsuo: evaluation of OFET, computational calculations, data curation, writing – review and editing; K. Naka: conceptualization, investigation, writing – review and editing, supervision; H. Imoto: conceptualization, investigation, writing – original draft, writing – review and editing, funding acquisition project administration, supervision.

Conflicts of interest

There are no conflicts to declare.

Acknowledgements

We thank Prof. Dr H. Yamada of Kyoto University for evaluating the OFET devices. This work was supported by the JST FOREST Program (Grant Number JPMJFR221K) to HI and a Grant-in-Aid for JSPS Fellows (Grant 23KJ1405) to AS.

Notes and references

1 (*a*) N. Tokitoh, *Acc. Chem. Res.*, 2004, **37**, 86; (*b*) N. Tokitoh, *Bull. Chem. Soc. Jpn.*, 2004, **77**, 429; (*c*) A. J. Ashe III, *Acc. Chem. Res.*, 1978, **11**, 153; (*d*) A. J. Ashe III, *Top. Curr. Chem.*, 1982, **105**, 125; (*e*) V. Y. Lee and A. Sekiguchi, *Organometallic Compounds of Low-Coordinate Si, Ge, Sn and Pb: From Phantom Species to Stable Compounds*, John Wiley & Sons, Ltd., Chichester, UK, 2010; (*f*) G. Märkl, *Angew. Chem.*, 1966, **78**, 907.

2 (*a*) N. T. Coles, A. Sofie Abels, J. Leitl, R. Wolf, H. Grützmacher and C. Müller, *Coord. Chem. Rev.*, 2021, **433**, 213729; (*b*) P. Le Floch, *Coord. Chem. Rev.*, 2006, **250**, 627; (*c*) P. Le Floch and F. Mathey, *Coord. Chem. Rev.*, 1998, **178–180**, 771; (*d*) C. Müller, L. E. E. Broeckx, I. de Krom and J. J. M. Weemers, *Eur. J. Inorg. Chem.*, 2013, **2013**, 187.

3 (*a*) K. Masada, K. Okabe, S. Kusumoto and K. Nozaki, *Chem. Sci.*, 2023, **14**, 8524; (*b*) K. Masada, S. Kusumoto and K. Nozaki, *Organometallics*, 2023, **42**, 971; (*c*) E. Yue, A. Petrov, D. S. Frost, L. Dettling, L. Conrad, F. Wossidlo, N. T. Coles, M. Weber and C. Müller, *Chem. Commun.*, 2022, **58**, 6148.

4 C. Müller, D. Wasserberg, J. J. M. Weemers, E. A. Pidko, S. Hoffmann, M. Lutz, A. L. Spek, S. C. J. Meskers, R. A. J. Janssen, R. A. van Santen and D. Vogt, *Chem.–Eur. J.*, 2007, **13**, 4548.

5 (*a*) R. Sugiyama, R. Okada, T. Noda, N. Meguro, N. Yoshida, K. Hoshi, H. Ohta, M. Hayashi, H. Sasabe and J. Kido, *Chem.–Eur. J.*, 2024, **30**, e202304328; (*b*) G. Pfeifer, F. Chahdoura, M. Papke, M. Weber, R. Szűcs, B. Geffroy, D. Tondelier, L. Nyulászi, M. Hissler and C. Müller, *Chem.–Eur. J.*, 2020, **26**, 10534; (*c*) U. Balijapalli, X. Tang, D. Okada, Y.-T. Lee, B. S. B. Karunathilaka, M. Auffray, G. Tumen-Ulzii, Y. Tsuchiya, A. S. D. Sandanayaka, T. Matsushima, H. Nakanotani and C. Adachi, *Adv. Opt. Mater.*, 2021, **9**, 210112; (*d*) X. Tang, U. Balijapalli, D. Okada, B. S. B. Karunathilaka, C. A. M. Senevirathne, Y. Lee, Z. Feng, A. S. D. Sandanayaka, T. Matsushima and C. Adachi, *Adv. Funct. Mater.*, 2021, **31**, 2104529; (*e*) N. Ledos, T. Sangchai, I. Knysh, M. H. E. Bousquet, P. Manzhi, M. Cordier, D. Tondelier, B. Geffroy, D. Jacquemin, P.-A. Bouit and M. Hissler, *Org. Lett.*, 2022, **24**, 6869.

6 (*a*) G. Märkl and K.-H. Heier, *Angew Chem. Int. Ed. Engl.*, 1972, **11**, 1017; (*b*) G. Märkl and K. H. Heier, *Tetrahedron Lett.*, 1974, **15**, 4501; (*c*) G. Märkl, A. Kallmünzer, H. Nöth and K. Pohlmann, *Tetrahedron Lett.*, 1992, **33**, 1597; (*d*) L. Zhang, F. Yang, G. Tao, L. Qiu, Z. Duan and F. Mathey, *Eur. J. Inorg. Chem.*, 2017, **2017**, 2355; (*e*) Y. Mei, D.-J. Wu, J. E. Borger and H. Grützmacher, *Angew. Chem., Int. Ed.*, 2018, **57**, 5512.

7 (*a*) H. G. de Graaf, J. Dubbeldam, H. Vermeer and F. Bickelhaupt, *Tetrahedron Lett.*, 1973, **14**, 2397; (*b*) H. G. de Graaf and F. Bickelhaupt, *Tetrahedron*, 1975, **31**, 1097; (*c*) K. H. Dçtz, A. Tiriliomis and K. Harms, *Tetrahedron*, 1993, **49**, 5577; (*d*) S. G. Ruf, J. Dietz and M. Regitz, *Tetrahedron*, 2000, **56**, 6259; (*e*) Y. Mao, K. M. H. Lim, R. Ganguly and F. Mathey, *Org. Lett.*, 2012, **14**, 4974.

8 F. Nief, C. Charrier, F. Mathey and M. Simalty, *Tetrahedron Lett.*, 1980, **21**, 1441.

9 (*a*) P. de Koe and F. Bickelhaupt, *Angew Chem. Int. Ed. Engl.*, 1967, **6**, 567; (*b*) P. de Koe, R. van Veen and F. Bickelhaupt, *Angew Chem. Int. Ed. Engl.*, 1968, **7**, 465; (*c*) P. de Koe and F. Bickelhaupt, *Angew Chem. Int. Ed. Engl.*, 1968, **7**, 889; (*d*) G. Jongsma, H. Vermeer, F. Bickelhaupt, W. Schäfer and A. Schweig, *Tetrahedron*, 1975, **31**, 2931; (*e*) P. de Koe and F. Bickelhaupt, *Z. Naturforsch., B: J. Chem. Sci.*, 2003, **58**, 782; (*f*) S. Ito, K. Koshino and K. Mikami, *Chem.–Asian J.*, 2018, **13**, 830.

10 (*a*) Y. Kobayashi, I. Kumadaki, A. Ohsawa and H. Hamana, *Tetrahedron Lett.*, 1976, **17**, 3715; (*b*) Y. Kobayashi, I. Kumadaki, A. Ohsawa and H. Hamana, *Tetrahedron Lett.*, 1976, **17**, 3715; (*c*) I. Begum, G. Schnakenburg, Z. Kelemen, L. Nyulászi, R. T. Boeré and R. Streubel, *Chem. Commun.*, 2018, **54**, 13555; (*d*) A. Gese, S. Kermanshahian, G. Schnakenburg, Z. Kelemen, L. Nyulaszi, A. E. Ferao and R. K. Streubel, *Inorg. Chem.*, 2021, **60**, 13029; (*e*) D. Rottschäfer, B. Neumann, H.-G. Stammler, T. Sergeieva, D. M. Andrada and R. S. Ghadwal, *Chem.–Eur. J.*, 2021, **27**, 3055.

11 (*a*) N. H. T. Huy, B. Donnadieu and F. Mathey, *Organometallics*, 2007, **26**, 6497; (*b*) N. H. T. Huy, B. Donnadieu and F. Mathey, *Organometallics*, 2008, **27**, 4005.

12 (*a*) R. C. Fischer and P. P. Power, *Chem. Rev.*, 2010, **110**, 3877; (*b*) K. Ota and R. Kinjo, *Chem. Soc. Rev.*, 2021, **50**, 10594.
13 A. J. Ashe III, *J. Am. Chem. Soc.*, 1971, **93**, 3293.
14 (*a*) G. Märkl, H. Hauptmann and D.-C. J. Advena, *Angew. Chem., Int. Ed.*, 1972, **11**, 441; (*b*) G. Markl and R. Liebel, *Angew. Chem., Int. Ed.*, 1974, **13**, 668; (*c*) G. Markl and S.-C. F. Kneidl, *Angew. Chem., Int. Ed.*, 1974, **13**, 667; (*d*) G. Markl, H. Baier and S. Heinrich, *Angew. Chem., Int. Ed.*, 1975, **14**, 710; (*e*) A. J. Ashe III and T. W. Smith, *J. Am. Chem. Soc.*, 1976, **98**, 7861; (*f*) G. Markl and R. Liebel, *Angew. Chem., Int. Ed.*, 1977, **16**, 637; (*g*) A. J. Ashe III and W.-T. Chan, *J. Org. Chem.*, 1979, **44**, 1409.
15 (*a*) P. Jutzi and K. Deuchert, *Angew Chem. Int. Ed. Engl.*, 1969, **8**, 991; (*b*) H. Vermeer and F. Bickelhaupt, *Angew Chem. Int. Ed. Engl.*, 1969, **8**, 992.
16 A. J. Ashe, X. Fang and J. W. Kampf, *Organometallics*, 2001, **20**, 2109.
17 V. Kremláček, M. Erben, R. Jambor, A. Růžička, J. Turek, E. Rychagova, S. Ketkov and L. Dostál, *Chem.–Eur. J.*, 2019, **25**, 5668.
18 D. Rottschäfer, T. Glodde, B. Neumann, H.-G. Stammler, D. M. Andrada and R. S. Ghadwal, *Angew. Chem., Int. Ed.*, 2021, **60**, 15849.
19 R. E. Messersmith, S. Yadav, M. A. Siegler, H. Ottosson and J. D. Tovar, *J. Org. Chem.*, 2017, **82**, 13440.
20 K. Matsuo, R. Okumura, H. Hayashi, N. Aratani, S. Jinnai, Y. Ie, A. Saeki and H. Yamada, *Chem. Commun.*, 2022, **58**, 13576.
21 A. Sumida, T. Onishi, H. Imoto and K. Naka, *Dalton Trans.*, 2024, **53**, 1706.
22 (*a*) L. Weber, *Chem. Ber.*, 1996, **129**, 367; (*b*) M. Driess, H. Pritzkow and M. Sander, *Angew Chem. Int. Ed. Engl.*, 1993, **32**, 283.
23 (*a*) Z. Chen, C. S. Wannere, C. Corminboeuf, R. Puchta and P. v. R. Schleyer, *Chem. Rev.*, 2005, **105**, 3842; (*b*) H. F.-B. Shaidaei, C. S. Wannere, C. Corminboeuf, R. Puchta and P. v. R. Schleyer, *Org. Lett.*, 2006, **8**, 863.
24 R. G.-. Poranne and A. Stanger, *Chem.–Eur. J.*, 2014, **20**, 5673.
25 D. Geuenich, K. Hess, F. Kçhler and R. Herges, *Chem. Rev.*, 2005, **105**, 3758.
26 D. Lungerich, O. Papaianina, M. Feofanov, J. Liu, M. Devarajulu, S. I. Troyanov, S. Maier and K. Amsharov, *Nat. Commun.*, 2018, **9**, 4756.
27 (*a*) M. W. Schmidt, P. N. Truong and M. S. Gordon, *J. Am. Chem. Soc.*, 1985, **109**, 5217; (*b*) P. v. R. Schleyer and D. Kost, *J. Am. Chem. Soc.*, 1988, **110**, 2105.
28 A. Bondi, *J. Am. Chem. Soc.*, 1964, **68**, 441.
29 (*a*) B. Jeziorski, R. Moszynski and K. Szalewicz, *Chem. Rev.*, 1994, **94**, 1887; (*b*) R. M. Parrish, L. A. Burns, D. G. A. Smith, A. C. Simmonett, A. E. DePrince, E. G. Hohenstein, U. Bozkaya, A. Y. Sokolov, R. Di Remigio, R. M. Richard, J. F. Gonthier, A. M. James, H. R. McAlexander, A. Kumar, M. Saitow, X. Wang, B. P. Pritchard, P. Verma, H. F. Schaefer, K. Patkowski, R. A. King, E. F. Valeev, F. A. Evangelista, J. M. Turney, T. D. Crawford and C. D. Sherrill, *J. Chem. Theory Comput.*, 2017, **13**, 3185.
30 A. Saeki, *Polym. J.*, 2020, **52**, 1307.
31 (*a*) Y. Tsutsui, T. Sakurai, S. Minami, K. Hirano, T. Satoh, W. Matsuda, K. Kato, M. Takata, M. Miura and S. Seki, *Phys. Chem. Chem. Phys.*, 2015, **17**, 9624; (*b*) K. Kranthiraja, M. Nomura, F. Ishiwari and A. Saeki, *J. Photopolym. Sci. Technol.*, 2022, **35**, 205.
32 Bottom-gate bottom-contact OFET devices of **3c** and **3d** were prepared by vacuum deposition. However, the deposited films were too rough, as observed by polarized optical microscopy, to measure reproducibly. This is likely due to the low molecular weight of **3c** and **3d**, which caused re-sublimation during vacuum deposition.
33 (*a*) N. Nakata, N. Takeda and N. Tokitoh, *J. Am. Chem. Soc.*, 2002, **124**, 6914; (*b*) N. Takeda, A. Shinohara and N. Tokitoh, *Organometallics*, 2002, **21**, 256; (*c*) Y. Mizuhata, N. Takeda, T. Sasamori and N. Tokitoh, *Chem. Lett.*, 2005, **34**, 1088; (*d*) T. Sasamori, K. Inamura, W. Hoshino, N. Nakata, Y. Mizuhata, Y. Watanabe, Y. Furukawa and N. Tokittoh, *Organometallics*, 2006, **25**, 3533; (*e*) Y. Mizuhata, S. Fujimori, N. Noda, S. Kanesato and N. Tokitoh, *Dalton Trans.*, 2018, **47**, 14436; (*f*) T. Ishii, K. Suzuki, T. Nakamura and M. Yamashita, *J. Am. Chem. Soc.*, 2016, **138**, 12787; (*g*) A. J. Ashe III, *J. Am. Chem. Soc.*, 1971, **93**, 6690; (*h*) A. J. Ashe III, T. R. Diephouse and M. Y. El-Sheikh, *J. Am. Chem. Soc.*, 1982, **104**, 5693; (*i*) A. J. Ashe III and M. D. Gordon, *J. Am. Chem. Soc.*, 1972, **94**, 7596; (*j*) G. Märkl and G. F. Lieb, *Angew. Chem., Int. Ed.*, 1968, **7**, 733; (*k*) A. J. Ashe and M. D. Gordon, *J. Am. Chem. Soc.*, 1972, **94**, 7596.
34 (*a*) W. Levason and G. Reid, in *Comprehensive Coordination Chemistry II*, ed. J. A. McCleverty and T. J. Meyer, Elsevier, Amsterdam, 2004, ch. 1.16, vol. 1, p. 384; (*b*) H. Kihara, S. Tanaka, H. Imoto and K. Naka, *Eur. J. Inorg. Chem.*, 2020, **2020**, 3662.
35 (*a*) R. A. Boto, F. Peccati, R. Laplaza, C. Quan, A. Carbone, J.-P. Piquemal, Y. Maday and J. Contreras-García, *J. Chem. Theory Comput.*, 2020, **16**, 4150; (*b*) E. R. Johnson, S. Keinan, P. Mori-Sánchez, J. C.-. García, A. J. Cohen and W. Yang, *J. Am. Chem. Soc.*, 2010, **132**, 6498.
36 (*a*) A. Hettche and K. Dimorth, *Chem. Ber.*, 1973, **106**, 1001; (*b*) K. Dimorth, *Phosphorus-Carbon Double Bonds*, Fortschritte der Chemischen Forschung, Springer, 1973.